DOI: 10.1002/fuce.201500203

First Principles Modeling of Pd-doped (La,Sr)(Co,Fe)O_3 Complex Perovskites

Yu. A. Mastrikov[1]*, S. Guo[2,3], F. Puleo[2], L. F. Liotta[2], E. A. Kotomin[1,4]

[1] Institute of Solid State Physics, University of Latvia, 8 Kengaraga str., Riga LV-1063, Latvia
[2] Institute for the Study of Nanostructured Materials (ISMS)-CNR, Palermo 90146, Italy
[3] Northwestern Polytechnical University, Xi'an 710072 PR China
[4] Max Planck Institute for Solid State Research, Heisenbergstr. 1, Stuttgart 70569, Germany

Received December 15, 2015; accepted January 08, 2016; published online March 15, 2016

Abstract

(La,Sr)(Co,Fe)O_3 (LSCF) perovskites are well known promising materials for cathodes of solid oxide fuel cells. In order to reduce cathode operational temperature, doping on *B*-sublattice with different metals was suggested. Indeed, as it was shown recently experimentally, doping with low Pd content increases oxygen vacancy concentration which is one of factors controlling oxygen transport in fuel cells. In this Communication, we modeled this material using first principles DFT calculations combined with supercell model. The charge density redistribution, density of states, and local lattice distortion around palladium ions are analyzed and reduction of the vacancy formation energy confirmed.

Keywords: Solide Oxide Fuel Cells, Cathode, (La,Sr)(Co,-Fe)O3, Pd-doping, Oxygen Vacancy, First Principal Calculations

1 Introduction

Environmentally friendly solid oxide fuel cells operated at intermediate temperatures, 800–1,000 K (IT-SOFC), are worldwide investigated for potentially high efficiency in energy conversion [1]. Currently, the two most promising cathode materials are (Ba,Sr)(Co,Fe)O_3 (BSCF) and (La,Sr)(Co,Fe)O_3 (LSCF) [2, 3]. BSCF shows better performance but has several shortcomings, including irreversible transformation into hexagonal phase and carbonate formation in CO_2-containing atmosphere. In turn, LSCF is more stable and thus, being further doped with metal on *B*-sublattice, could serve as a promising candidate for IT-SOFC cathode. Till now, LSCF doped by Pd, Ag, Pt, Cu, etc. have been investigated [4–8]. As is well understood [2, 3], the cathode performance is largely controlled by the oxygen vacancy formation and migration energies. It was shown recently [9] that an increase of the oxygen vacancy concentration, which is known to improve cathode performance, could be effectively achieved even with low Pd content, if some part is stabilized as cationic dopants into the perovskite lattice and the remaining part is in the form of metallic nanoparticles. In this Communication, we report the results of first principles calculations of LSCF doped with Pd. The charge density redistribution, density of states, and local lattice distortion around impurities are analyzed and their effect on the oxygen vacancy formation energy discussed.

2 Method and Model

Calculations were performed using DFT method, as implemented in the computer code VASP 5.3 [10] in conjunction with the projector-augmented method (PAW) and plane wave basis set [11]. Core electrons were treated by means of the ultrasoft pseudopotentials (Table 1), the PBE exchange-correlation functional was of the GGA-type [12]. We would like to stress here that based on our experience [2, 3, 13, 14], the GGA approximation reliably reproduces the basic structural and electronic properties of complex perovskites and related compounds, except for the underestimated band gaps in the insulating states of parent perovskites, e.g. $LaMnO_3$. A detailed study of the latter perovskite has clearly shown a perfect agreement between calculated atomic structure and its ground anti-ferromagnetic state with experimental data, including formation enthalpy [15]. This is confirmed by a very good agreement between calculated and experimental heat of formation of brownmillerite-type $SrFeO_{2.5}$ from parent oxides, SrO and Fe_2O_3 [16]. On the other hand, the use of GGA+*U* approximation is hardly possible for the LSCF under study, since it contains several types of magnetic ions (Fe, Co, Pd) and thus

[*] *Corresponding author, yuri.mastrikov@cfi.lu.lv*

needs optimization of several Hubbard-U parameters. Moreover, LSCF is a metal and thus usual fitting of the U-parameter to the band gap is impossible here. Lastly, we focus in this paper on the trend in vacancy formation energy upon LSCF doping which is not sensitive to the electron correlation effects.

The plane-wave basis set was determined by the cut-off energy of $520\times1.6\ 10^{-19}$ J. The Brillouin zone was sampled by the Monkhorst-Pack scheme $4\times4\times4$ [17]. Defect-free structures were fully optimized ($a_0=3.84\times10^{-10}$m for LSCF and $a_0=3.87\times10^{-10}$m for LSCFP). After the introduction of oxygen vacancy only atomic position optimization was performed, with the lattice parameters kept fixed. Additional tests have shown that lattice relaxation gain at such a low vacancy concentration does not exceed $0.04\times1.6\ 10^{-19}$ J per unit cell. The effective charge analysis was performed, using the Bader method [18]. Our dopant calculations are based on the supercell approach successfully used in previous study [13] for vacancy formation in $La_{0.5}Sr_{0.5}Co_{0.5}Fe_{0.5}O_3$.

Thus, the model $La_{0.5}Sr_{0.5}Co_{0.5}Fe_{0.25}Pd_{0.25}O_3$ supercell comprises eight ABO_3 formula units (Figure 1). A-type cations (La and Sr) are arranged strictly alternating analogous to the rock salt structure, whereas Fe and Pd cations, separated by the largest possible distance within the supercell, $a_0\sqrt{3}$, correspond to the bcc sublattice. 24 oxygen ions can be discriminated by the type of nearest B-cations: Co, Fe and Pd. Three types of oxygen vacancies $V_O^{\bullet\bullet}$ can be created, respectively: Co-$V_O^{\bullet\bullet}$-Co, Co-$V_O^{\bullet\bullet}$-Fe, and Co-$V_O^{\bullet\bullet}$-Pd. As shown in Fig.1, each type of oxygen vacancy is located at the particular distance from the Pd dopant: six Co-$V_O^{\bullet\bullet}$-Pd-type vacancies are located at $a_0/2$, twelve Co-$V_O^{\bullet\bullet}$-Co-type vacancies – at $a_0\sqrt{5}/2$, and six Co-$V_O^{\bullet\bullet}$-Fe-type vacancies – at $a_03/2$. The positions of Fe and Pd cations are mutually reciprocal. So, any Co-$V_O^{\bullet\bullet}$-Co-type vacancy is always at the same distance from Fe and Pd cations.

Replacement of one from two Fe atoms by Pd ions in 40 atom supercell leads to 12.5% B-sublattice doped compound. This is much larger than in real experiments but done on purpose to recognize doping effects in a most pronounced way. Oxygen vacancies were created by removing one neutral atom from a supercell (resulting in nonstoichiometry of $ABO_{3-\delta}$, $\delta=0.125$), see more details in [13]. There are two types of vacancies in the undoped LSCF structure – Co-$V_O^{\bullet\bullet}$-Co and Co-$V_O^{\bullet\bullet}$-Fe whose concentrations are equal, whereas in 12.5% Pd doped structures we have 50% of Co-$V_O^{\bullet\bullet}$-Co, 25% of Co-$V_O^{\bullet\bullet}$-Fe and 25% of Co-$V_O^{\bullet\bullet}$-Pd (Figure 1). As shown earlier for undoped LSCF, $V_O^{\bullet\bullet}$ formation energy depends considerably on the type of its two nearest cations (Co–Co or Co–Fe). When we calculate below the average vacancy formation energies, we use the fractional concentrations mentioned above as weighting factors.

Table 1 Electronic configuration and cut-off energy of used US pseudopotentials with the PAW method applied [11].

Element	Valence states	Cut-off energy/$1.6\ 10^{-19}$ J
La	$5s^25p^66s^25d^1$	219.313
Sr	$4s^24p^65s^2$	229.282
Co	$4s^13d^8$	267.969
Fe	$3p^64s^13d^7$	293.238
Pd	$4p^65s^14d^9$	271.098
O	$2s^22p^4$	400.000

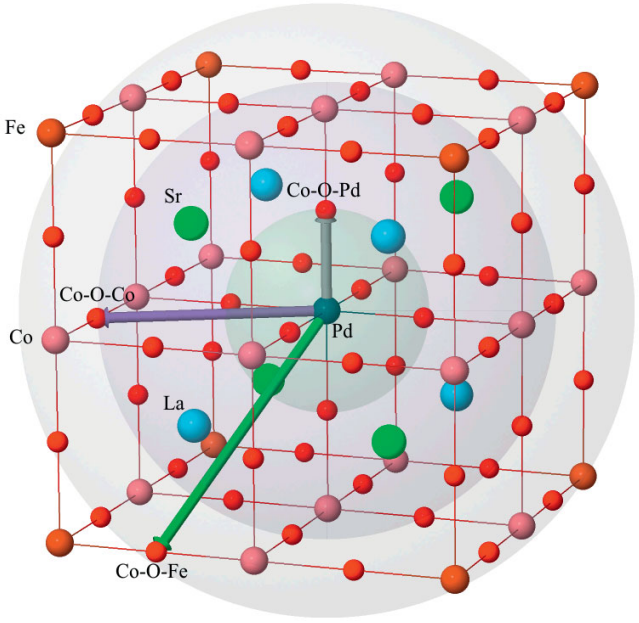

Fig. 1 A supercell of modeled $La_{0.5}Sr_{0.5}Co_{0.5}Fe_{0.25}Pd_{0.25}O_3$ structure. Three nonequivalent types of oxygen positions are indicated: Co–O–Pd (25%), Co–O–Co (50%), Co–O–Fe (25%).

3 Results and Discussion

It was shown earlier [13] that $V_O^{\bullet\bullet}$ formation energy near Co is smaller than near Fe ion. In doped LSCF, as one can see from Table 2, the vacancies nearest to Pd show the formation energies ~10% smaller than Co-$V_O^{\bullet\bullet}$-Co ones in the Pd-free material. The Co-$V_O^{\bullet\bullet}$-Co and Co-$V_O^{\bullet\bullet}$-Fe vacancies more remote from Pd dopants also show the reduced energies, typically 5%. Comparing the average values, one can clearly see that Pd doping effectively ($\sim0.17\times1.6\ 10^{-19}$ J) decreases single vacancy formation energy, and thus, increases $V_O^{\bullet\bullet}$ equilibrium concentration, in agreement with [9]. (The effect should be weaker for smaller dopant concentrations in real experiments.)

In our calculations, the lattice oxygen ion has an effective charge of $-1.1\times1.6\ 10^{-19}$ C only, much smaller than the formal charge of $-2\times1.6\ 10^{-19}$ C, which indicates a considerable covalency in the B-O chemical bonding well established in ABO_3 perovskites. After removal of a neutral O atom from the supercell, this charge gets redistributed: about two thirds of it go to the B-cations nearest to the vacancy, whereas the rest is redistributed between more remote B-cations.

Table 2 Oxygen vacancy formation energy in Pd-doped LSCF (in 1.6 10^{-19} J) calculated with respect to the 1/2 O_2 molecule in a gas phase. The calculated O_2 binding energy is 5.24 × 1.6 10^{-19} J.

$V_O^{\bullet\bullet}$ formation energy, $\delta = 0.125$	Co-$V_O^{\bullet\bullet}$-Co	Weight	Co-$V_O^{\bullet\bullet}$-Fe	Weight	Co-$V_O^{\bullet\bullet}$-Pd	Weight	Average
$La_{0.5}Sr_{0.5}Co_{0.75}Fe_{0.25}O_{3-\delta}$ [15]	2.64	0.5	2.81	0.5			2.72
$La_{0.5}Sr_{0.5}Co_{0.75}Fe_{0.125}Pd_{0.125}O_{3-\delta}$	2.52	0.5	2.80	0.25	2.38	0.25	2.55

For Co-$V_O^{\bullet\bullet}$-Co and Co-$V_O^{\bullet\bullet}$-Fe vacancies the charge redistribution in undoped and doped LSCF remains practically the same, regardless of the doping (Table 3): –0.34 × 1.6 10^{-19} C from a removed O atom go to Co and –0.30 × 1.6 10^{-19} C to Fe. For the Pd-doped system the additional charge on Co in the Co-$V_O^{\bullet\bullet}$-Pd complex is slightly smaller, –0.32 × 1.6 10^{-19} C. Simultaneously, in the Co-$V_O^{\bullet\bullet}$-Pd vacancy one observes a strong extra charge localization (–0.4*e*) on Pd.

The calculated magnetic moments on the cations confirm previous conclusions on the high spin configuration of Fe and intermediate spin on Co [13]. In contrast, the magnetic moment on Pd is small, its effective charge is also smaller than that for a nominally 3+ ion, thus we assign it as the low-spin Pd^{2+} (d^8) ions. The presence of palladium cations in the perovskite lattice is in agreement with previous results [9] and as well with experimental studies on Pd in other oxides where Pd^{2+} (and or Pd^{4+}) species were detected [19–21].

The electronic density of states (DOS) projected onto different elements is plotted in Figure 2. Since it is hard to compare directly the energies for perfect and defective systems, we aligned the energy scales, in order to match the deep O 2*s* core states (thin vertical line), similarly to our previous studies [14]. As one can see, the electrons left upon oxygen removal move the Fermi level upward (dotted red line). The DOS for Co ions overlaps with the Fermi energy whereas that for Fe shows a gap of ca. 1 × 1.6 10^{-19} J. This is why electrons of a removed O atom prefer to move more towards nearest Co ions rather Fe. Projections onto Co, Fe and O upon Pd doping are similar to those for Pd-free LSCF. In the Pd-doped system shown here, there is also a considerable Pd-DOS crossing the Fermi level and thus electrons are expected to be easily localized on Pd ions, in agreement with the charge redistribution above discussed (Table 2).

The difference maps for the electronic charge density are shown in Figure 3. They clearly demonstrate charge density redistribution from the oxygen vacancy over two nearest cations, as observed earlier in Pd-free BSCF and LSCF [2, 3, 13], whereas several nearest ions are slightly polarized. In other words, $V_O^{\bullet\bullet}$ produces rather local distortion of the crystalline lattice. These maps confirm the effective atomic charge analysis above that doping does not affect the charge distribution within the Co-$V_O^{\bullet\bullet}$-Co and Co-$V_O^{\bullet\bullet}$-Fe complexes, however, much larger charge density is concentrated on Pd next to the vacancy than on a regular Co ion where charge on Co ions on the opposite side of the vacancy, in its turn, is reduced.

Oxygen vacancy formation in cubic-type ABO_3 perovskites breaks the -*B*-O-*B*- structural chain, causing certain structure distortion accompanied with the outward displacements of the two *B*-type nearest-neighbor (NN) cations, whereas four 2NN oxygen ions, from each of two nearest to the vacancy BO_2-planes, move inwards. Usually, these are the most pronounced atomic displacements induced by the vacancy. Without Pd doping, 2NN oxygen ions are displaced typically by 0.16–0.18 × 10^{-10} m, i.e. ~ 5% of the lattice constant. In turn, displacements of NN *B*-cations are smaller, by a factor of 4–5. In the doped systems the atomic relaxation pattern strongly depends on the type of doping and the type of vacancy. Thus, in Co-$V_O^{\bullet\bullet}$-Co complex in Pd-doped LSCF we found that the *B*-cations are stronger displaced outwards (0.14 × 10^{-10} m) than oxygen ions inwards (0.10–0.12 × 10^{-10} m) (with respect to perfect crystalline sites). Moreover, Pd cations show the Jahn-Teller distortion with different Pd–O distances in the *x*, *y* and *z* directions of 2.04 and 2.06 × 10^{-10} m, which confirms its attribution to the low-spin d^8 configuration (The small effect could be related to high defect concentration and their interaction in nearest

Table 3 Electron charge redistribution and magnetic moments on *B*-cations in LSCF. The atomic effective charges *q* and charge deviation Δ*q* (in 1.6 × 10^{-19} C) with respect to defect-free LSCF, magnetic moments M on Co, Fe, Pd (in 9.27 × 10^{-24} J T^{-1}) are shown.

$La_{0.5}Sr_{0.5}Co_{0.75}Fe_{0.25}O_{3-\delta}$	bulk			Co-$V_O^{\bullet\bullet}$-Co		Co-$V_O^{\bullet\bullet}$-Fe			
		q	M	Δ*q*	M	Δ*q*	M		
	Co	1.57	1.53	–0.34	1.40	–0.34	1.50		
	Fe	1.67	2.92			–0.30	2.97		
$La_{0.5}Sr_{0.5}Co_{0.75}Fe_{0.125}Pd_{0.125}O_{3-\delta}$	bulk			Co-$V_O^{\bullet\bullet}$-Co		Co-$V_O^{\bullet\bullet}$-Fe		Co-$V_O^{\bullet\bullet}$-Pd	
		q	M	Δ*q*	M	Δ*q*	M	Δ*q*	M
	Co	1.58	1.71	–0.34	1.52	–0.35	1.52	–0.32	1.75
	Fe	1.67	3.06			–0.30	3.04		
	Pd	1.47	0.20					–0.40	0.01

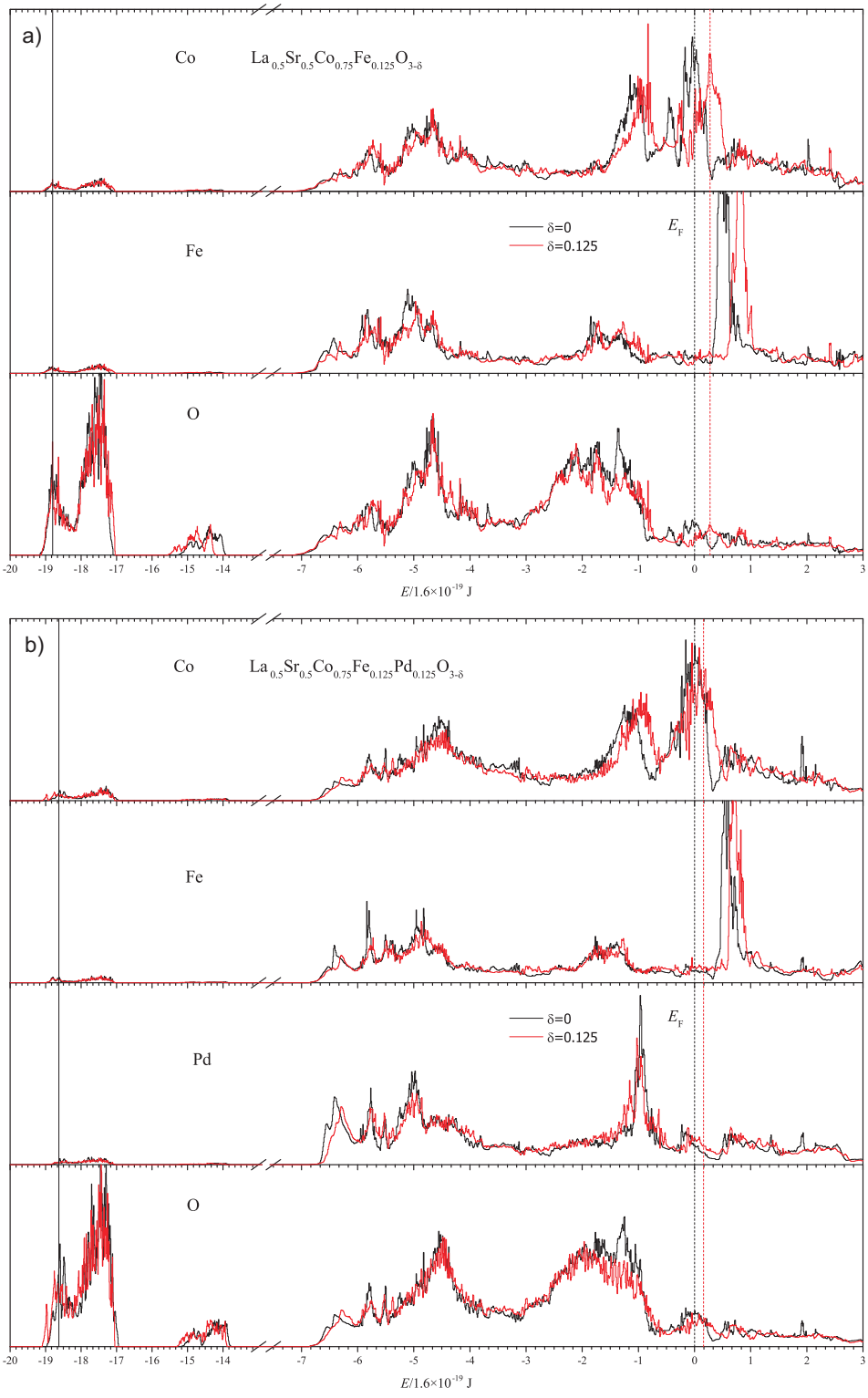

Fig. 2 Projected Co, Fe, Pd and O density of states for stoichiometric ($\delta = 0$) and non-stoichiometric ($\delta = 0.125$) LSCF – undoped (a) and doped with Pd (b). The energy scale was adjusted to align the deep O 2*s* states (thin solid vertical line), dashed lines indicate the Fermi energy E_F (taken as zero for the stoichiometric in oxygen system).

supercells, similarly to the Fe^{4+} case in $SrTiO_3$ [22]). Keeping in mind the Shannon O^{2-} ion radius 1.4×10^{-10} m, the Pd radius could be estimated as 0.64×10^{-10} m, again in agreement with that expected for Pd^{2+} in many oxides [23]. Note that these Pd–O distances are typical for many perovskites [20].

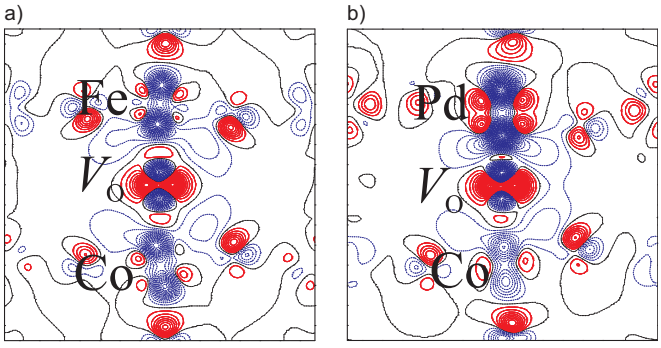

Fig. 3 Difference electron density maps for oxygen vacancy in Pd-doped LSCF (the total electron density of defective system minus that for the perfect one) in two different vacancy configurations –Co-$V_O^{\bullet\bullet}$-Fe (a) and Co-$V_O^{\bullet\bullet}$-Pd (b) (Table 2). Solid red and dash blue isolines correspond to deficiency and excess of electron density, respectively. Dash-dotted black line marks the zero level. Isolines increment $-0.02 \times 1.6\ 10^{11}$ C m^{-3}.

4 Conclusions

Our calculations on $La_{0.5}Sr_{0.5}Co_{0.75}Fe_{0.125}Pd_{0.125}O_{3-\delta}$ suggest the presence of low-spin Pd^{2+} and clearly show a decrease of oxygen vacancy formation energy. These results are in agreement with previous experimental findings for two compositions, $La_{0.6}Sr_{0.4}Co_{0.8}Fe_{0.17}Pd_{0.03}O_{3-\delta}$ and $La_{0.6}Sr_{0.4}Co_{0.2}Fe_{0.77}Pd_{0.03}O_{3-\delta}$, where cationic palladium species stabilized into the perovskite lattice were detected. Considerable electronic density redistribution and atomic structure local distortion around palladium ions contribute to the reduced formation energy. Further calculations modeling the effect of dopant Pd cation clustering are in progress.

Acknowledgements

Research has been performed within the framework of COST Action CM 1104, STSM (COST-STSM-ECOST-STSM-CM1104-010414-042095), and EC GREEN-CC (grant agreement 608524). S. Guo thanks China Scholarship Council for financial support. Authors thank R. Merkle, J. M. Serra, E. Antipov for numerous discussions.

References

[1] D. J. L. Brett, A. Atkinson, N. P. Brandon, S. J. Skinner, *Chem. Soc. Rev.* **2008**, *37*, 1568.
[2] E. A. Kotomin, R. Merkle, Yu. A. Mastrikov, M. M. Kuklja, J. Maier, in *Computational Approaches to Energy Materials* (Eds. A. Walsch, A. Sokol, C. R. A. Catlow), Wiley **2013**, p. 149.
[3] M. M. Kuklja, E. A. Kotomin, R. Merkle, Yu. A. Mastrikov, J. Maier, *Phys. Chem. Chem. Phys.* **2013**, *15*, 5443.
[4] C. Sun, R. Hui, J. Roller, *J. Solid State Electrochem.* **2010**, *14*, 1125.
[5] T. Huang, X. Shen, C. Chou, *J. Power Sources* **2009**, *187*, 348.
[6] J. Chen, F. Liang, B. Chi, J. Pu, S. Jiang, L. Jian, *J. Power Sources* **2009**, *194*, 275.
[7] J. A. Kilner, M. Burriel, *Ann. Rev. Mater. Res.* **2014**, *44*, 365.
[8] J. M. Serra, H. P. Buchkremer, *J. Power Sources* **2007**, *72*, 768.
[9] F. Puleo, L. F. Liotta, V. la Parola, D. Banerjee, A. Martorana, A. Longo, *PhysChemChemPhys.* **2014**, *16*, 22677.
[10] G. Kresse, J. Hafner, *Phys. Rev. B* **1993**, *47*, 558.
[11] G. Kresse, J. Joubert, *Phys. Rev. B* **1999**, *59*, 1758.
[12] J. P. Perdew, K. Burke, M. Ernzerhof, *Phys. Rev. Lett.* **1996**, *77*, 3865.
[13] Yu. A. Mastrikov, R. Merkle, E. A. Kotomin, M. M. Kuklja, J. Maier, *PhysChemChemPhys.* **2013**, *15*, 911.
[14] E. A. Kotomin, Yu. A. Mastrikov, M. M. Kuklja, R. Merkle, A. Roytburd, J. Maier, *Solid State Ionics* **2011**, *188*, 1.
[15] E. A. Kotomin, R. A. Evarestov, Yu. A. Mastrikov, J. Maier, *PhysChemChemPhys.* **2005**, *7*, 2346.
[16] D. Fuks, Yu. Mastrikov, E. A. Kotomin, J. Maier, *J. Mater. Chem. A* **2013**, *1*, 14320.
[17] H. J. Monkhorst, J. D. Pack, *Phys. Rev. B* **1976**, *13*, 5188.
[18] W. Tang, E. Sanville, G. Henkelman, *J. Phys.: Condens. Matter* **2009**, *21*, 084204.
[19] R. V. Panin, N. R. Khasanova, C. Bougerol, W. Schnelle, G. van Tendeloo, E. V. Antipov, *Inorganic Chemistry Comm.* **2010**, *49*, 1295.
[20] A. Eyssler, P. Mandaliev, A. Winkler, P. Hug, O. Safonova, R. Figi, A. Weidenkaff, D. Ferri, *J. Phys. Chem. C* **2010**, *114*, 4594.
[21] J. P. Attfield, *Acta Cryst. B* **1988**, *44*, 563.
[22] V. E. Alexandrov, R. A. Evarestov, E. A. Kotomin, J. Maier, *J. Phys.: Conf. Ser.* **2008**, *117*, 012001.
[23] R. D. Shannon, *Acta Cryst. A* **1976**, *32*, 751.